Fusion Engineering and Design 219 (2025) 115201

Contents lists available at ScienceDirect

Fusion Engineering and Design

journal homepage: www.elsevier.com/locate/fusengdes

Self-consistent equilibrium and transport simulations for NSTX-U plasmas enhanced via machine learning surrogate models

Brian Leard [a,*], Tariq Rafiq [a], Ian Ward [a], Franco Galfrascoli [a], Eugenio Schuster [a], Alexei Pankin [b], Marina Gorelenkova [b]

[a] *Mechanical Engineering and Engineering Mechanics, Lehigh University, Bethlehem, PA, USA*
[b] *Princeton Plasma Physics Laboratory, Princeton, NJ, USA*

ARTICLE INFO

Keywords:
Plasma confinement
Equilibrium and transport modeling
Machine learning
NSTX-U

ABSTRACT

The Control-Oriented Transport SIMulator (COTSIM) is an advanced equilibrium and transport code designed for simulating tokamak discharges at computational speeds suitable for control applications. COTSIM's modular framework enables users to select models that balance accuracy with speed according to specific needs, allowing the code to operate from fast to faster-than-real-time performance levels. This work presents recent enhancements to COTSIM's predictive accuracy for NSTX-U scenarios, achieved by integrating neural-network-based surrogate models and self-consistent equilibrium calculations. To improve source deposition predictions, a surrogate model for NUBEAM has been incorporated. Additionally, a surrogate model for the Multi-Mode Module (MMM) now supports predictions of anomalous thermal, momentum, and particle diffusivities—key factors for modeling the evolution of temperature and rotation. Each surrogate model was specifically trained for the NSTX-U operational regime to enhance COTSIM's accuracy while maintaining computational efficiency. Moreover, COTSIM now couples fixed-boundary equilibrium solvers with its transport solvers, enabling self-consistent predictions of plasma profiles and equilibrium evolution over the discharge. Simulation results demonstrate strong agreement between COTSIM and TRANSP predictions for NSTX-U discharges. These substantial advancements expand COTSIM's utility in model-based control applications for NSTX-U. Potential applications include simultaneous optimization of equilibrium and transport scenarios, integration into digital twins, real-time profile estimation (e.g., temperature and rotation) from limited or noisy measurements, and advanced feedback-based scenario control.

1. Introduction

Future tokamaks, like ITER, aim to achieve advanced plasma states characterized by higher plasma energy. At these elevated energies, disruptions could cause severe heat loads on the plasma-facing components, limiting the experimental flexibility enjoyed by current-generation tokamaks when exploring the parameter space. Consequently, there is an increasing need to thoroughly understand novel tokamak scenarios before experimental testing to mitigate the risk of plasma instabilities leading to disruptions. In addition, tight control and highly effective disruption mitigation techniques are essential. Since this level of control must be accomplished with limited diagnostic, model-based estimators and synthetic diagnostics are crucial for monitoring the plasma state during operation.

To meet the needs of future tokamaks, several software tools have gained attention. Scenario planners use plasma dynamics models coupled with optimization algorithms to determine optimal actuator trajectories for achieving desired tokamak scenarios [1–4]. Since scenario planning typically requires numerous simulations to effectively explore the parameter space, generally plasma simulation codes with shorter computation times are preferred. However, the accuracy of the simulation code determines the effectiveness of the resulting solution. Digital twins in the fusion context are full three-dimensional recreations of the entire tokamak environment, illustrating how engineering design impacts machine operation [5,6]. Applications for digital twins range from estimating plasma properties in experimental discharges with limited diagnostics to discharge planning and future fusion pilot plant (FPP) design. Often digital twins are integrated modeling frameworks that couple various codes for different physical processes and regions of the tokamak. Both scenario planners and digital twins benefit from incorporating plasma simulation codes that are fast, modular, and user-friendly. Scenario planners, as mentioned, often require many simulations, and a code with lengthy computation times can make

* Corresponding author.
E-mail address: brl220@lehigh.edu (B. Leard).

https://doi.org/10.1016/j.fusengdes.2025.115201
Received 17 January 2025; Received in revised form 26 April 2025; Accepted 18 May 2025
Available online 12 June 2025

optimization intractable or limit the scope to a reduced number of parameters. Likewise, extended calculation times restrict the applications of a digital twin, making real-time estimation or between-shot analysis impractical and slowing the overall pace of research.

A modular design offers a way to balance speed and accuracy by integrating models of varying complexity, allowing users to select the optimal model for specific requirements. This approach not only enables flexibility in computational speed and accuracy but also allows the code to be evaluated against itself for validation purposes. Moreover, a segmented code with an intuitive workflow and user-friendly interface facilitates integration within larger suites, whether for scenario optimization, digital twins, or tokamak PCS, and makes the code more accessible to new users. One code that embodies many of these benefits is the Control-Oriented Tokamak SIMulator (COTSIM). COTSIM is a MATLAB-based, modular, 1.5D, equilibrium and transport code that was initially developed in [7] for synthesizing feedback profile controllers in both conventional and spherical tokamaks [8–10]. To achieve the necessary speed for control applications, early versions of COTSIM used half-dimensional, control-oriented models for temperature, density, and auxiliary sources, with plasma equilibrium assumed constant.

Since then, COTSIM has been expanded to include transport equations for electron and ion temperatures as well as toroidal rotation [11], with additional transport equations continuously being added. Neural-network surrogate models were integrated in [12,13] to emulate computationally intensive codes, improving accuracy while preserving COTSIM's fast computation times required for control. COTSIM has been successfully incorporated into scenario planners for DIII-D [3], EAST [14], and NSTX-U [4], and has also been used for state estimation [15]. Recently, three different analytical equilibrium solvers have been integrated with COTSIM's transport equations to enable self-consistent transport and equilibrium simulations with a time-evolving equilibrium. These solvers can be used interchangeably and offer varying tradeoffs in terms of accuracy and speed, a specific example of COTSIM's modularity. In this work, we present the latest modeling additions to COTSIM and compare its simulation results with predictive TRANSP runs for an NSTX-U scenario, demonstrating close agreement in plasma parameter predictions with significantly reduced computation times. These fast computation times, combined with COTSIM's modular and intuitive design, make it a strong candidate for a variety of applications such as scenario planners and digital twins.

2. Plasma equilibrium modeling in COTSIM

2.1. Analytical solution to the GSE

The plasma magnetic equilibrium can be modeled using the cylindrical coordinate system (R, Z, ϕ). By assuming toroidal axisymmetry the equilibrium can be represented by the well-known Grad-Shafranov Equation (GSE), [16,17],

$$R\frac{\partial}{\partial R}\left(\frac{1}{R}\frac{\partial\psi}{\partial R}\right)+\frac{\partial^2\psi}{\partial Z^2}=-\mu_0 R J_\phi(R,Z) \tag{1}$$

$$J_\phi(R,Z)=R\frac{\partial p}{\partial\psi}+\frac{f}{\mu_0 R}\frac{\partial f}{\partial\psi}, \tag{2}$$

where $\psi(R,Z)$ is the poloidal magnetic flux, $J_\phi(R,Z)$ is the toroidal current density, μ_0 is the permitivity of free space, and p is the plasma pressure. The toroidal field function is defined as $f = RB_t$, where $B_t(R,Z)$ is the toroidal magnetic field [18]. As indicated by (2), J_ϕ is physically dependent on $\psi(R,Z)$, making the GSE a nonlinear elliptic PDE . While this type of equation can be difficult to solve analytically, previous work such as [19,20], and [21] have done so by assuming J_ϕ takes the form of a given function, thus constraining the right hand side of the equation. Separation of variables can then be employed to produce a general analytic solution to the GSE with various unknown constants. These constants are then solved for using boundary conditions imposed at the last closed flux surface, which are derived from the major radius R_0, the minor radius a, the elongation κ, and the triangularity δ. Additional constraints related to the plasma current I_p and poloidal beta β_p are further imposed. Solving the system of equations produced by these constraints yields the full analytical equation for the two-dimensional poloidal flux map, $\psi(R,Z)$.

COTSIM is embedded with three solvers that find the solution to the GSE analytically. Each follows the general analytical method discussed in the previous paragraph, but have different particulars in technique. Throughout this work, these analytical solvers will be referred to as Equilibrium Solver 1, 2, and 3, and are respectively based on the analytical methods presented in [19,20], and [21]. Each of these analytical solvers simplify the GSE by assuming the form of the toroidal current density, J_ϕ. The first two, Equilibrium Solver 1 and 2, assume that J_ϕ can be represented by the function that takes the general form,

$$J_\phi(R)=-\frac{1}{\mu_0}(C_1 R-\frac{C_2}{R}), \tag{3}$$

where C_1 and C_2 are constants determined by solving the boundary condition and β_p, I_p, constraints. Notably this function is only dependent on the R coordinate. A comparison of (2) and (3) makes evident that $C_1 = -\mu_0(\partial p/\partial\psi)$ and $C_2 = f(\partial f/\partial\psi)$. By substituting (3) back into the GSE (1), it is possible to split the solution $\psi(R,Z)$ into homogeneous and particular parts satisfying the left and right side of the GSE, respectively. The homogeneous solution takes the form of a polynomial series truncated after a chosen number of terms. Equilibrium Solver 1 uses the analytical method in [19], which demonstrated this technique for a limited, horizontally symmetric plasma. The approach used by Equilibrium Solver 2, shown in [20], builds off [19] by truncating the polynomial series at a higher order term which yields a more versatile analytical function that is constrained by additional boundary conditions. Equilibrium Solver 2 also normalizes the (R,Z) coordinate system by the major radius R_0 and is suitable for limited, single, or double null plasmas. Equilibrium Solver 3, based on the method in [21], constrains the toroidal current slightly differently,

$$J_\phi(R,Z)=\psi(R,Z)(C_3 R+\frac{C_4}{R}), \tag{4}$$

where the variables C_3 and C_4 are constants. While the second term is similar to (3), now $J_\phi(R,Z)$ is a 2D variable due to the dependence on $\psi(R,Z)$. Note that a comparison of (2) and (4) shows that $C_3 = (\partial p/\partial\psi)/\psi$ and $C_4 = f(\partial f/\partial\psi)/(\mu_0\psi)$. After changing the coordinate system and separating variables, a general analytical solution is found in the form of a trigonometric series, and once again free parameters are determined via boundary conditions. Like Equilibrium Solver 2, Equilibrium Solver 3 includes solutions suited for both limited and diverted plasma types.

As mentioned earlier, each of these solvers use I_p and β_p to impose constraints on the analytical solution and solve for $\psi(R,Z)$. COTSIM considers the plasma current I_p as an input, and β_p is calculated as follows,

$$\beta_p=\frac{\beta_t B_{t,0}^2}{B_{p,0}^2}, \tag{5}$$

where $B_{t,0}$ and $B_{p,0}$ are the toroidal and poloidal magnetic fields at the major radius R_0. The poloidal magnetic field at R_0 can be computed by,

$$B_{p,0}=\frac{\mu_0 I_p}{P_b}, \tag{6}$$

where P_b is the circumference of the last closed flux surface, considered the plasma boundary. The variable β_t is the toroidal beta, one of the global parameters computed by COTSIM that is discussed in Section 3.5.

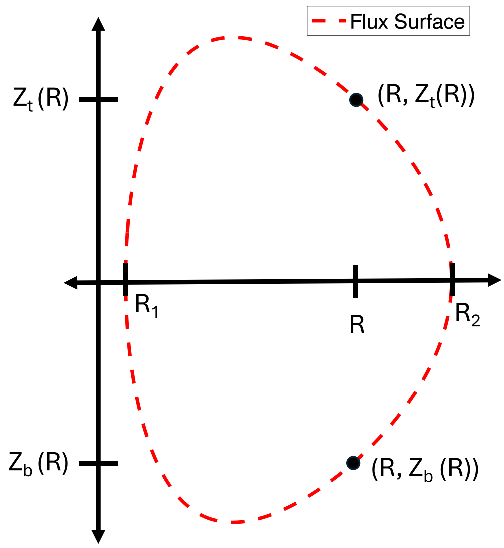

Fig. 1. Notable coordinates on a given flux surface.

2.2. Computing equilibrium parameters

The transport equations in COTSIM assume that plasma properties are constant on each nested flux surface. This allows the flux surface to act as a spatial coordinate for plasma properties, and the tokamak environment can be reduced to 1D, i.e. a given property $X(R,Z)$ becomes $X(\psi)$. COTSIM uses the effective minor radius to index flux surfaces,

$$\rho = \sqrt{\frac{\Phi}{\pi B_{t,0}}}. \tag{7}$$

The variable Φ is the toroidal magnetic flux, defined as,

$$\Phi(\psi) = \int_{A(\psi)} B_t dA, \tag{8}$$

where $A(\psi)$ is the area of the flux surface with the constant value of $\psi(R,Z)$. This can be expressed as,

$$A(\psi) = \int_{R_1(\psi)}^{R_2(\psi)} [Z_t(\psi,R) - Z_b(\psi,R)]dR, \tag{9}$$

where the variables $R_1(\psi)$ and $R_2(\psi)$ are the minimum and maximum R coordinates of the flux surface, and $Z_t(\psi,R)$ and $Z_b(\psi,R)$ are the top and bottom Z coordinate of the flux surface at a specific R position. These coordinates are labeled in Fig. 1. By substituting (8) and (9) into (7) and using the definition of f, it is possible to solve for $\rho(\psi)$,

$$\rho(\psi) = \sqrt{\frac{1}{\pi B_{t,0}} \int_{R_1}^{R_2} \frac{f(\psi)}{R}(Z_t(\psi,R) - Z_b(\psi,R))dR}. \tag{10}$$

Note that these analytical solvers assume that $f(\psi)$ is constant on flux surfaces. The 2D coordinate grid (R,Z), is now mapped to a 1D spatial coordinate indexed by ρ. Finally, this coordinate is normalized,

$$\hat{\rho} = \rho/\rho_b, \in \{0,1\} \tag{11}$$

where ρ_b is the effective minor radius of the plasma boundary.

The poloidal flux map $\psi(R,Z)$ is also used to compute several other equilibrium parameters that are included in the transport equations in Section 3. The major and minor radius of each flux surface, $R_0^\psi(\hat{\rho})$, and $a_\psi(\hat{\rho})$ are found using,

$$R_0^\psi(\hat{\rho}) = \frac{R_1(\hat{\rho}) + R_2(\hat{\rho})}{2}, \tag{12}$$

$$a_\psi(\hat{\rho}) = \frac{R_2(\hat{\rho}) - R_1(\hat{\rho})}{2}. \tag{13}$$

Note that now $\hat{\rho}$ and not ψ is being used to index the flux surface. The volume of each flux surface is determined via the equation,

$$V(\hat{\rho}) = 2\pi \int_{R_1}^{R_2} R\left(Z_t(\hat{\rho}) - Z_b(\hat{\rho})\right) dR. \tag{14}$$

The normalized equilibrium parameters $\hat{F}(\hat{\rho})$, $\hat{G}(\hat{\rho})$, and $\hat{H}(\hat{\rho})$ are defined as follows,

$$\hat{F} \triangleq \frac{R_0 B_0}{f(\hat{\rho})}, \quad \hat{G} \triangleq \left\langle \frac{R_0^2}{R^2}|\nabla\rho|^2 \right\rangle, \quad \hat{H} \triangleq \frac{\hat{F}(\hat{\rho})}{\langle R_0^2/R^2\rangle}, \tag{15}$$

where the symbols $\langle\rangle$ denote a flux surface average. As shown in [22], flux averaged values can be written as,

$$\langle X\rangle(\hat{\rho}) = \frac{\int_P \frac{X}{B_p} dl}{\int_P \frac{1}{B_p} dl}, \tag{16}$$

where $X(R,Z)$ is a generalized 2D value. The variable $P(\hat{\rho})$ is the contour of the flux surface and l is a differential unit vector along P. Therefore,

$$\left\langle R_0^2/R^2\right\rangle(\hat{\rho}) = R_0^2 \frac{\int_P \frac{1}{R^2 B_p} dl}{\int_P \frac{1}{B_p} dl}, \tag{17}$$

The poloidal magnetic field is determined from the flux map,

$$B_p(R,Z) = \frac{1}{R}\nabla\psi \times \hat{e}_\phi = \frac{1}{R}\sqrt{\left(\frac{\partial\psi}{\partial R}\right)^2 + \left(\frac{\partial\psi}{\partial Z}\right)^2}, \tag{18}$$

where $\hat{e}_\phi$ is the toroidal unit vector. After substituting (18) into (17) and finding $\hat{F}$, it is possible to solve for $\hat{H}$. The parameter $\hat{G}$ is determined by transforming the gradient of ρ,

$$|\nabla\rho|^2 = \left(\frac{\partial\rho}{\partial\psi}\right)^2 |\nabla\psi|^2 = \left(\frac{\partial\rho}{\partial\psi}\right)^2 \left[\left(\frac{\partial\psi}{\partial R}\right)^2 + \left(\frac{\partial\psi}{\partial Z}\right)^2\right], \tag{19}$$

which allows $\hat{G}$ to be written as,

$$\hat{G}(\hat{\rho}) = R_0^2 \left(\frac{\partial\rho}{\partial\psi}\right)^2 \frac{\int_P B_p dl}{\int_P 1/B_p dl}. \tag{20}$$

The equilibrium parameters can now be calculated given the flux $\psi(R,Z)$, R_0, and B_0.

Figs. 2 and 3 show comparisons of the computed equilibrium profiles between each of the discussed analytical equilibrium solvers and TRANSP, which computes the equilibrium using the fixed-boundary code TEQ [23]. The analytical solver inputs, i.e. R_0, a, κ, δ, I_p, and β_p were taken from NSTX-U experimental shot 204 985 at t = 1.1 s. As shown by Fig. 2(a), $J_\phi(\hat{\rho})$ calculated using Equilibrium Solver 1 and 2 has significant variation with TRANSP due to the assumptions made by (3). In contrast, Equilibrium Solver 3 matches TRANSP's J_ϕ fairly well. Because of this, Equilibrium Solver 3 has the closest matching to TRANSP for the other equilibrium profiles, with no profile showing significant deviation. Even with the J_ϕ mismatch, Equilibrium Solver 1 and 2 are able to match TRANSP for many of the other equilibrium profiles. However, Equilibrium Solver 1 underpredicts $\hat{F}$, $\hat{H}$, and R_0^ψ, and has a flatter $\hat{G}$ profile. Equilibrium Solver 2 shows a mismatch with $\hat{F}$ and overpredicts $\hat{H}$ toward the core, but otherwise matches TRANSP approximately as well as Equilibrium Solver 3.

3. Plasma transport modeling in COTSIM

COTSIM contains several one-dimensional transport models. It converts continuous transport PDE's to a discrete series of ODE's by using the finite differences method, and operates with a fixed-time-step. Transport equations can be run either implicitly, explicitly, or hybrid, with initial conditions established by the user.

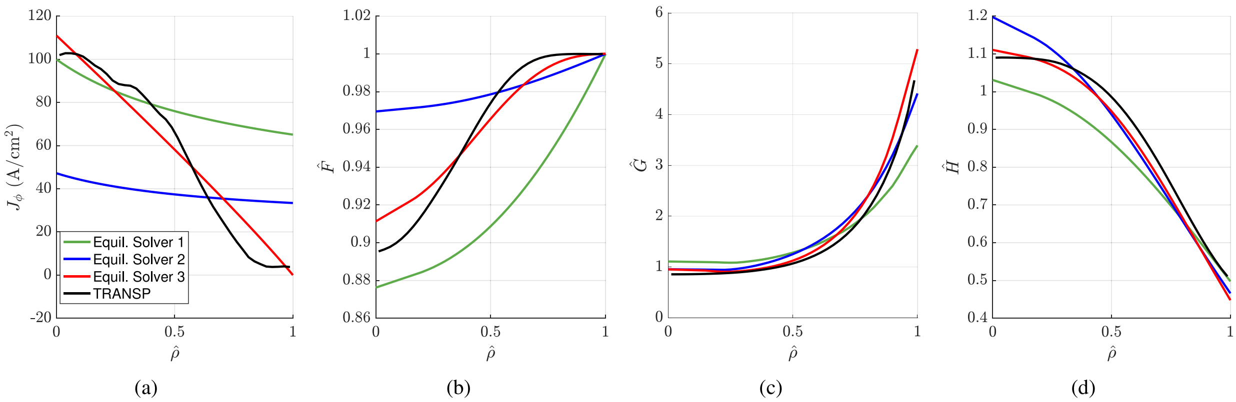

Fig. 2. Comparison of J_ϕ and the normalized equilibrium profiles $\hat{F}$, $\hat{G}$, and $\hat{H}$ calculated using each of COTSIM's analytical equilibrium solvers and a TEQ equilibrium. The shape parameters, I_p, and β_p were taken from NSTX-U experimental shot 204 985 at $t = 1.1$ s.

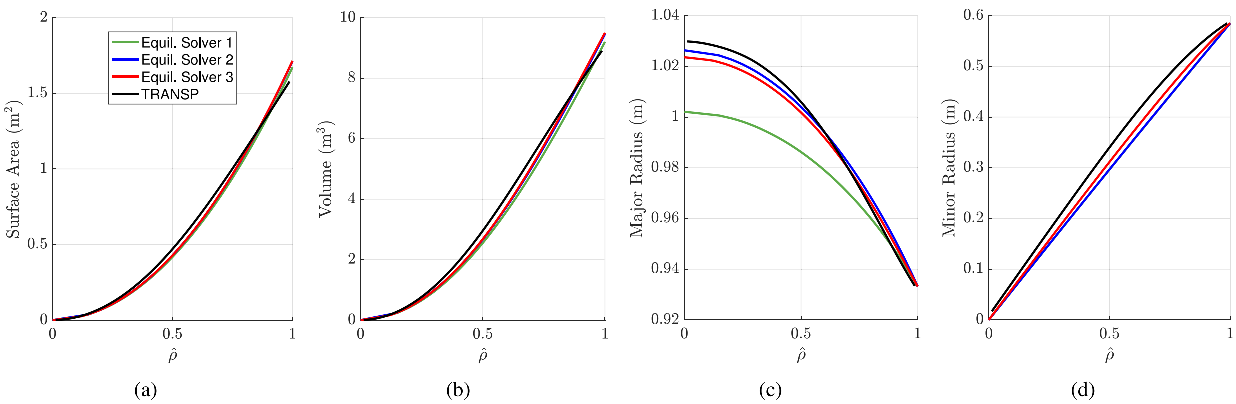

Fig. 3. Comparison of S, V, R_0^ψ, and a_ψ calculated using each of COTSIM's analytical equilibrium solvers and TRANSP.

3.1. Magnetic diffusion equation

The poloidal magnetic flux evolution is governed by the magnetic diffusion equation (MDE), derived from Gauss's law, Ampere's law, and the MHD momentum equation [24]. This equation can be written as,

$$\frac{\partial \psi}{\partial t} = \frac{\eta(T_e)}{\mu_0 {\rho_b}^2 \hat{F}^2} \frac{1}{\hat{\rho}} \frac{\partial}{\partial \hat{\rho}} \left(\hat{\rho} \hat{F} \hat{G} \hat{H} \frac{\partial \psi}{\partial \hat{\rho}} \right) + \eta(T_e) R_0 \hat{H} J_{ni}, \quad (21)$$

$$\left.\frac{\partial \psi}{\partial \hat{\rho}}\right|_{\hat{\rho}=0} = 0, \quad \left.\frac{\partial \psi}{\partial \hat{\rho}}\right|_{\hat{\rho}=1} = -k_{I_p} I_p(t), \quad (22)$$

where $\eta(t,\hat{\rho})$ is the plasma resistivity, $T_e(t,\hat{\rho})$ is the electron temperature, and $J_{ni}(t,\hat{\rho})$ is the noninductive current deposition, which is composed of the auxiliary current J_{aux} and the bootstrap current J_{bs}. In this work, it is assumed that the auxiliary current comes solely from neutral beam injection, $J_{aux} = J_{nb}$. This is modeled using a neural-network surrogate model for NUBEAM [25], further discussed in Section 4. The bootstrap current is calculated using the Sauter model detailed in [26]. The plasma resistivity η is computed from the simplified Spitzer model shown in [8]. The parameter k_{I_p} that factors into the boundary condition at the plasma edge is another equilibrium parameter, mathematically defined as $k_{I_p} \triangleq \mu_0 R_0/(2\pi \hat{G}(1)\hat{H}(1))$.

The safety factor profile is inversely related to the spatial derivative of the poloidal magnetic flux,

$$q(t,\hat{\rho}) = -\frac{B_{t,0}\rho_b^2 \hat{\rho}}{\theta(t,\hat{\rho})}, \quad (23)$$

where $\theta(t,\hat{\rho}) \triangleq \partial\psi/\partial\hat{\rho}$. This parameter measures the magnetic pitch and is related to the magneto-hydrodynamic stability of the plasma.

3.2. Heat transport equation

The temperature evolution for a general species (either electron or ion) is dictated by the heat transport equation (HTE) [27], which can be expressed as,

$$\frac{3}{2}\frac{\partial}{\partial t}(n_{e,i}T_{e,i}) = \frac{1}{\rho_b^2 \hat{H} \hat{\rho}} \frac{\partial}{\partial \hat{\rho}} \left[\hat{\rho} \frac{\hat{G}\hat{H}^2}{\hat{F}} (\chi_{e,i} n_{e,i}) \frac{\partial T_{e,i}}{\partial \hat{\rho}} \right] + Q_{e,i}, \quad (24)$$

$$\left.\frac{\partial T_{e,i}}{\partial \hat{\rho}}\right|_{\hat{\rho}=0} = 0, \quad T_{e,i}(\hat{\rho}_{ped}) = T_{e,i}^{ped}, \quad (25)$$

where $T_{e,i}$ is the temperature of the electron/ion species, and similarly $n_{i,e}$ is the species density, $\chi_{e,i}$ is the diffusivity, and $Q_{e,i}$ is the heat deposition. It is important to note that for H-mode plasmas this equation is only valid in the core region, with the temperature of the pedestal being computed separately. The outer boundary condition is set by the pedestal location and height, $\hat{\rho}_{ped}$ and $T_{e,i}^{ped}$.

While COTSIM does have 0D and 1D transport equations for the density evolution, in this work the density of each species is computed using a simplified half-dimensional model,

$$n_{e,i}(\hat{\rho},t) = n_{e,i}^{prof}(\hat{\rho})\bar{n}_{e,i}(t), \quad (26)$$

where is $n_{e,i}^{prof}$ is a constant profile, often taken from an experimental time slice, and $\bar{n}_{e,i}$ is the line averaged density.

3.3. Thermal electron and ion diffusivities

The species diffusivities $\chi_{e,i}$ are composed of neoclassical and anomalous contributions,

$$\chi_{e,i} = \chi_{e,i}^{nc} + \chi_{e,i}^{an}, \quad (27)$$

where $\chi_{e,i}^{nc}$ is the neoclassical diffusivity and $\chi_{e,i}^{an}$ is the anomalous diffusivity due to various turbulent modes. The neoclassical diffusivity is calculated using the Chang-Hinton model [28], and the anomalous contribution is calculated using a surrogate model for the Multi-mode Module (MMM) [29], further discussed in Section 4. It is also possible to include the paleoclassical diffusivity, χ_e^{pal} [30,31], in the electron diffusivity calculation.

3.4. Heat sources

The electron and ion heat depositions for a non-burning plasma are composed of the following sources,

$$Q_e = Q_e^{ohm} - Q_e^{rad} - Q_{ie}^{coll} + Q_e^{nb}, \tag{28}$$
$$Q_i = Q_{ie}^{coll} + Q_i^{nb}, \tag{29}$$

where Q_e^{ohm} is the ohmic heating, Q_e^{rad} is the radiative heat loss, Q_{ie}^{coll} is the ion-electron collisional heating, and Q_e^{nb} and Q_i^{nb} are the beam heating sources to electrons and ions, respectively.

The ohmic heating is computed as,

$$Q_e^{ohm} = \eta {J_\phi}^2, \tag{30}$$

where the variable $J_\phi(\hat{\rho}, t)$ is the total toroidal ohmic current density. This can be expressed as,

$$J_\phi(\hat{\rho}, t) = -\frac{1}{\mu R_0 \rho_b^2 \hat{H}} \frac{1}{\hat{\rho}} \frac{\partial}{\partial \hat{\rho}} \left(\hat{\rho} \hat{G} \hat{H} \frac{\partial \psi}{\partial \hat{\rho}} \right), \tag{31}$$

which is notably similar to the first term of the MDE (21). The ohmic heating is one of the ways that the kinetic and magnetic profile evolutions are coupled.

The radiative heating is assumed to be dominated by Bremsstrahlung radiation, modeled as

$$Q_e^{rad} = k_{brem} Z_{eff} n_e^2 \sqrt{T_e}, \tag{32}$$

where $k_{brem} = 5.5 \times 10^{-37}$ W m$^3 \sqrt{\text{keV}}^{-1}$ is the Bremsstrahlung radiation coefficient and Z_{eff} is the effective charge of the plasma. The ion-electron collisional heating is determined by the equation,

$$Q_{ie}^{coll} = \frac{3n_e}{2\tau_{ei}}(T_e - T_i), \tag{33}$$

where τ_{ei} is the energy relaxation time, which is mathematically defined in [32] and explained in [33]. The neutral beam heating, Q_e^{nb} and Q_i^{nb}, are calculated using a neural network surrogate model for NUBEAM [25], further discussed in Section 4.

3.5. Global plasma parameters

Advanced tokamak scenarios are often characterized by global variables such as fusion gain, greenwald fraction, magnetic shear, and, for burning plasmas, power gain Q and net power produced. To determine if the spherical tokamak is a desirable concept for fusion energy production, one goal of NSTX-U is to achieve a high β_N [34]. Additionally, due to small aspect ratio tokamaks having less room in the center stack for ohmic coils, spherical tokamaks like NSTX-U seek to generate a significant portion of non-inductive current drive, f_{ni} [35]. Therefore it would be beneficial to predict both β_N and f_{ni} while planning NSTX-U scenarios. To calculate β_N, it is first necessary to compute the plasma thermal energy,

$$W = \int_0^1 \frac{\partial V}{\partial \hat{\rho}} \left(T_e n_e + T_i n_i \right) d\hat{\rho}. \tag{34}$$

The toroidal beta, β_t is a measure of the plasma internal pressure and the external pressure imposed by the toroidal magnetic field,

$$\beta_t = \frac{\mu_0 \left(W + \int_0^1 \frac{\partial V}{\partial \hat{\rho}} p_{fi} d\hat{\rho} \right)}{2 B_t^2 V(1)}, \tag{35}$$

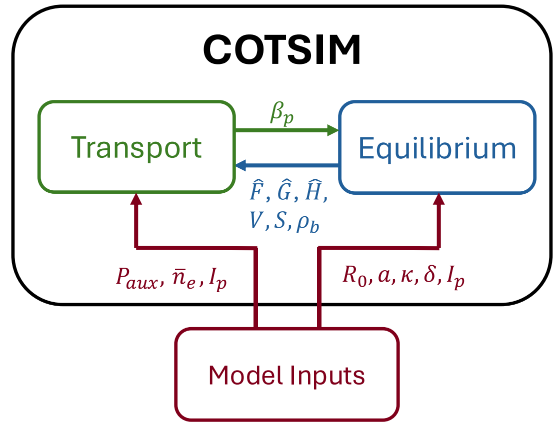

Fig. 4. The passing of variables between the transport solver and the equilibrium solver in COTSIM.

where $V(1)$ is the total volume of the plasma found by solving (14) at the plasma boundary, and p_{fi} is the fast ion pressure computed from NUBEAMNet. This value is then often normalized as follows,

$$\beta_N = \frac{\beta_t}{I_p/(a B_{t,0})}. \tag{36}$$

The noninuctive current fraction is a measure of the percentage of total plasma current that is not generated by the ohmic coil,

$$f_{ni} = \frac{1}{I_p} \int_0^1 \frac{\partial A}{\partial \hat{\rho}} (J_{nb} + J_{bs}) d\hat{\rho}. \tag{37}$$

Fig. 4 shows the passing of variables between the equilibrium and transport solvers in COTSIM. At each timestep the analytical equilibrium solver computes the 2D magnetic flux, which is used to calculate the equilibrium profiles discussed in Section 2.2. These profiles are then used in the 1D equations discussed in this section that evolve various plasma profiles and scalars for the next timestep. At the subsequent timestep, the updated β_p, I_p, and plasma boundary shape parameters (R_0, a, κ, δ) are used to recompute the 2D flux. Note that since temperature, density, and the fast ion pressure influence β_p and hence the equilibrium, the plasma equilibrium and transport are fully coupled. The auxiliary power P_{aux} and a density input (in this work $\bar{n}_e$) are inputs to the transport solver. The boundary shape parameters are inputs to the fixed-boundary equilibrium solver and the plasma current is a shared input to both the equilibrium and transport solvers.

4. Neural-network-based surrogate models

As mentioned, COTSIM has incorporated several neural-network surrogate models to recreate the results of physics-based codes without the associated long computational times. This has improved COTSIM's prediction accuracy while maintaining reasonable computation speeds. The surrogate models detailed in this work have been trained using TRANSP runs based on shots from the NSTX-U 2016 run campaign, and are therefore machine specific. Similar surrogate models have been created for DIII-D [12] and EAST [13].

MMMNet [29] is a surrogate model for the Multi-mode Module (MMM), a one-dimensional turbulent transport module that calculates the thermal, particle, and momentum diffusivities, [36–38]. MMMNet was trained on a database of over 500,000 time slices taken from approximately 600 TRANSP runs that predicted anomalous diffusivities using MMM version 9.1. The data was preprocessed by removing non-physical outliers, smoothing output profiles, and normalizing input and output values. Six separate two-layer, 120 node per layer networks were trained for each of the six anomalous diffusivities, with the inputs to each network being identical to MMM. This network has

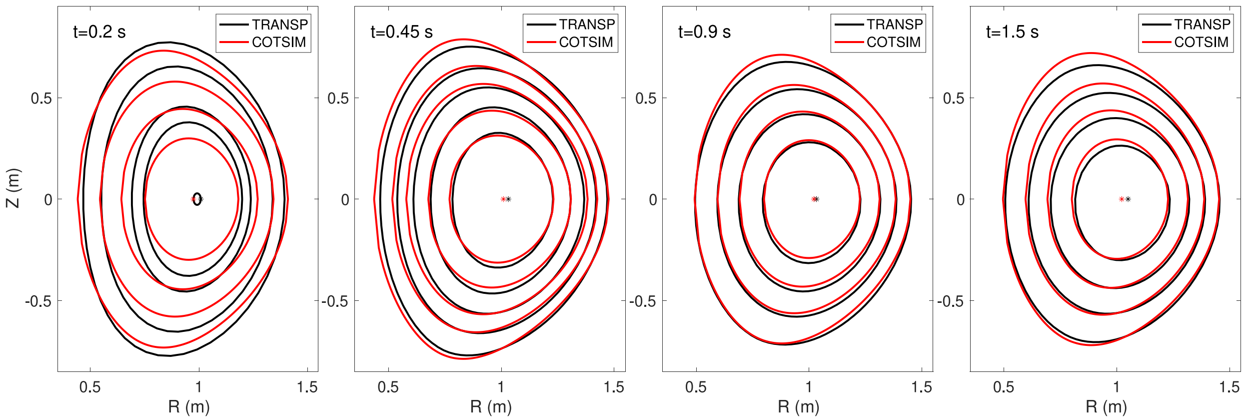

Fig. 5. Poloidal flux contours for TRANSP and COTSIM for various times throughout the simulated NSTX-U discharge.

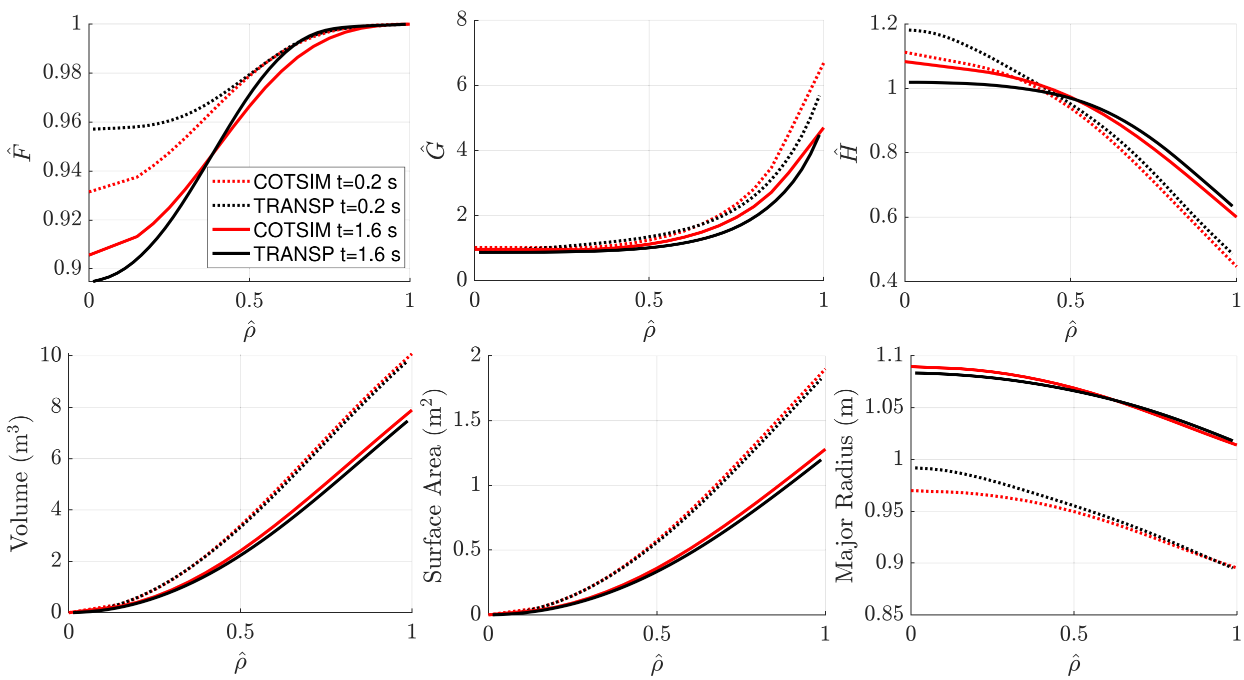

Fig. 6. Comparison of plasma equilibrium profiles at $t = 0.2$ s and $t = 1.6$ s.

been embedded in COTSIM to calculate the anomalous electron and ion thermal diffusivities, χ_e^{an} and χ_i^{an}, and future efforts will expand its uses to rotation and density prediction.

NUBEAMNet, first presented in [25], is a surrogate model for NUBEAM, a Monte-Carlo code that predicts the impact of neutral beam injection on the plasma [39,40]. NUBEAMNet is made up of three networks trained on a database of 100,000 time slices from approximately 1000 TRANSP runs. Principle component analysis was used to reduce the dimensionality of profiles and the beam powers were passed through a low pass filter to account for the impact of recent beam injection on the plasma state. This network has been embedded in COTSIM and is used to calculate the beam current deposition (j_{nb}) used in the MDE (21), the beam heating depositions (Q_e^{nb} and Q_i^{nb}) used in the HTE (24), and the fast ion pressure (p_{fi}) used in (35).

5. COTSIM validation for an NSTX-U scenario

COTSIM's predictions of the plasma state have been validated against TRANSP, an established 1.5D transport code that combines various physics models to provide a comprehensive picture of the plasma evolution in a tokamak discharge [41]. TRANSP was designed to be able to either predict plasma values or take them from experimental data depending on the needs of the user. In order to make one-to-one comparisons between plasma models in TRANSP and COTSIM, TRANSP predicts the electron and ion temperature as well as the safety factor profile, and the plasma equilibrium is computed using the fixed-boundary code TEQ. Additionally, the Chang-Hinton model solves for the neoclassical diffusivities, the anomalous diffusivities are predicted using MMM, the Spitzer model calculates the plasma resistivity, and the Sauter model is used for bootstrap current. These specific models were chosen to correspond with equivalent models used by COTSIM (or a neural-network surrogate). However, it is important to note that COTSIM makes certain simplifications in the implementation of these models to reduce computation time.

A predictive TRANSP run and an equivalent COTSIM simulation were conducted based on the NSTX-U experimental shot 204 149 from the 2016 run campaign. The initial profiles, plasma current I_p, NBI actuator power trajectories P_{aux}, and boundary shape parameters, R_0, a κ, and δ, were all taken from the experimental shot. The experimental temperature pedestal was used for both the TRANSP and COTSIM simulations. COTSIM was run with a timestep of 0.01 s, 21 spatial

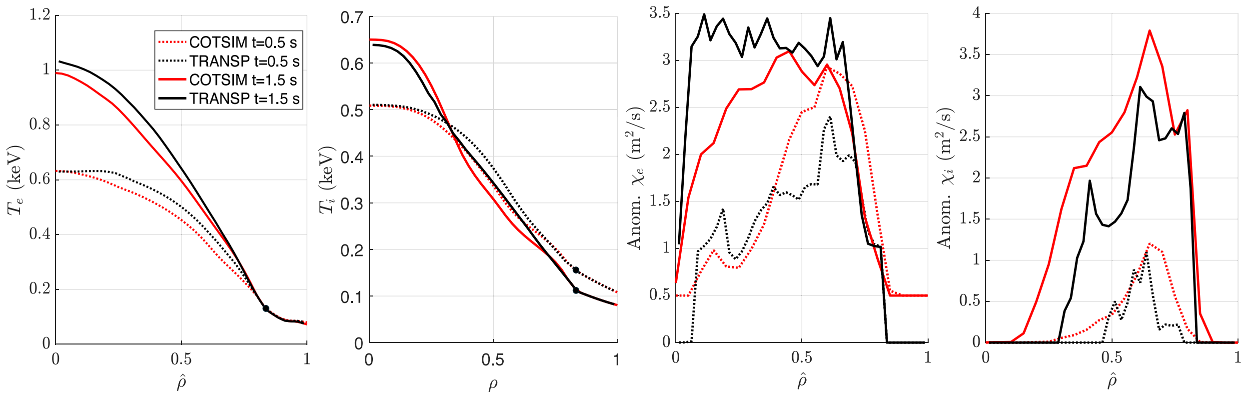

Fig. 7. Comparison of electron and ion temperatures and anomalous diffusivities at $t = 0.5$ s and $t = 1.5$ s.

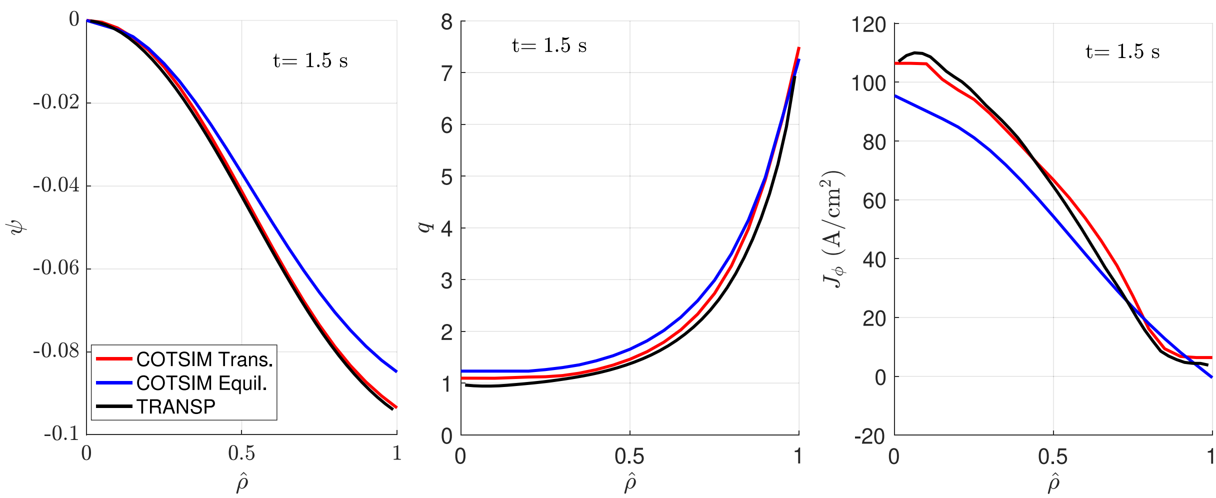

Fig. 8. Comparison of Magnetic flux, safety factor profile, and toroidal current profile at $t = 1.5$ s.

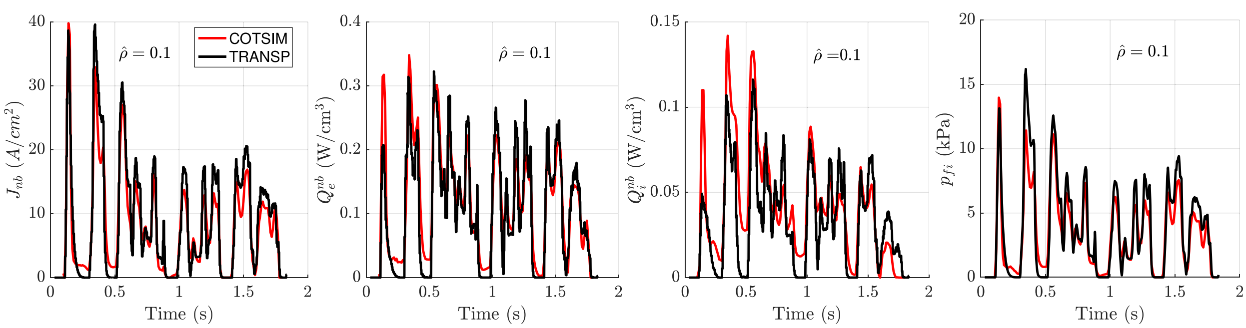

Fig. 9. Comparisons of NBI current, electron and ion heating, and fast ion pressure depositions between TRANSP and COTSIM at $\hat{\rho} = 0.1$.

nodes, and a hybrid numerical scheme. Equilibrium Solver 3 was used to calculate the plasma magnetic equilibrium.

Fig. 5 shows the 2D flux map $\psi(R, Z)$ at several times throughout the shot. While there is some deviation at $t = 0.2$ s, at each of the subsequent times there is fairly good matching between TRANSP and COTSIM. The equilibrium profiles for TRANSP and COTSIM are presented in Fig. 6, demonstrating how COTSIM is able to recreate TRANSP's profiles for significantly different equilibria. Similarly, Fig. 7 shows how COTSIM is able to recreate TRANSP's electron and ion temperature profiles using MMMNet to predict the anomalous thermal diffusivities. These results demonstrate that COTSIM+MMMNet remains accurate over an extended simulation time and does not diverge from the TRANSP+MMM solution. Note that the black dots in the temperature plots indicate the position of the pedestal. As mentioned, in this study COTSIM only solved for the core temperature.

Throughout a COTSIM simulation, various profiles are computed both via transport equations and within the equilibrium solver. These profiles are shown in Fig. 8, with the red line indicating the profile calculated via a transport equation and the blue line indicating a profile computed within the equilibrium solver. While there is a differentiation in these profiles, this was expected due to the different assumptions made by the equilibrium/transport solvers, such as those discussed in Section 2. Despite this, however, there is fairly good agreement in the profiles, indicating a reasonable degree of self-consistency within COTSIM. Furthermore, the profiles computed via the transport equations show a strong matching to those computed by TRANSP. Ultimately, COTSIM considers the transport profiles the official prediction. Fig.

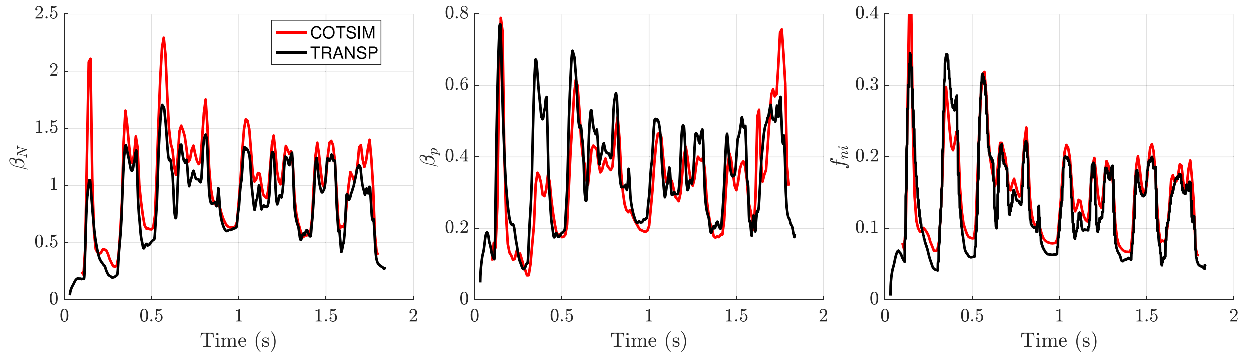

Fig. 10. Comparison of global plasma parameters β_N, β_p, and f_{ni} between TRANSP and COTSIM.

Table 1
Computation times of each analytical equilibrium solver embedded in COTSIM.

Equilibrium solver	Solver 1	Solver 2	Solver 3
Comp. time (s)	0.033	0.031	0.101
COTSIM time (s)	9.54	9.01	20.81

9 displays the NBI current, heating, and fast ion depositions at $\hat{\rho} = 0.1$.The NBI current deposition peaks approximately at $\hat{\rho} = 0.1$ while the heating and fast ion depositions peak on-axis. COTSIM with NUBEAM-Net demonstrates good agreement to TRANSP with NUBEAM. The trajectories for the global plasma parameters β_N and f_{ni} are presented in Fig. 10. COTSIM predicts a slightly higher β_N than TRANSP, partly due to periods of over-prediction in NBI heating. Conversely, the β_p computed by COTSIM is often slightly lower than TRANSP because COTSIM calculates a larger value of $B_{p,0}$. The non-inductive current fraction f_{ni} calculated by COTSIM is closely comparable to TRANSP.

COTSIM is able to perform these simulations on relatively short time scales. As mentioned, COTSIM has been designed to be flexible in terms of speed and accuracy trade-offs. COTSIM's modular design with alternative models of varying complexities allows the user to find a balance in accuracy and computation time depending on their needs. Similarly, the timestep and the 2D and 1D grid sizes offer speed/accuracy trade-offs. Computation times for this work are listed in Table 1. The first row lists the average time of a given analytical equilibrium solver, while the second row lists the total time of an NSTX-U simulation using that solver. Equilibrium Solvers 1 and 2 have comparable computation times, while Equilibrium Solver 3 is approximately three times longer due to the additional complexity of the analytical method. Each COTSIM simulation had a total of 171 timesteps with the equilibrium recomputed at each timestep. Since the equilibrium calculation is often the majority of the total computation, it is possible to significantly reduce simulation times by only updating the equilibrium after a given number of timesteps throughout the discharge. In comparison, predictive TRANSP runs are often several hours long. Summing up, COTSIM is able to simulate a time-varying NSTX-U discharge with close to the prediction accuracy of TRANSP while maintaining reasonably quick computation times.

6. Conclusion

COTSIM is a 1.5D transport code that simulates a fully integrated plasma equilibrium and transport evolution for a tokamak discharge. It has a modular design and intuitive workflow that allows the user to easily vary the model complexity and numerical grid size to find an appropriate balance between accuracy and speed. COTSIM has transport equations for the poloidal flux and the electron/ion temperature, which are supplemented with several neural-network surrogate models that predict the anomalous diffusivities and the NBI current and heating depositions. COTSIM also has three embedded fixed-boundary analytical equilibrium solvers that calculate the 2D poloidal flux map, yielding a fully integrated transport-equilibrium simulation of the plasma. COTSIM has been verified against TRANSP, which demonstrates that it can predict NSTX-U plasma scenarios with a close degree of accuracy, while reducing the computation time several orders of magnitude. COTSIM's combination of accuracy and speed, along with the modular and intuitive design of the code, make it uniquely suited for future integration within larger code suites such as scenario planners or full digital twins of the tokamak environment.

CRediT authorship contribution statement

Brian Leard: Writing – review & editing, Writing – original draft, Visualization, Validation, Resources, Methodology, Investigation, Formal analysis, Data curation, Conceptualization. **Tariq Rafiq:** Writing – review & editing, Software, Resources, Methodology, Investigation, Formal analysis, Data curation, Conceptualization. **Ian Ward:** Writing – review & editing, Methodology, Investigation. **Franco Galfrascoli:** Writing – review & editing, Investigation. **Eugenio Schuster:** Writing – review & editing, Resources, Project administration, Funding acquisition, Formal analysis, Conceptualization. **Alexei Pankin:** Software, Resources, Data curation. **Marina Gorelenkova:** Software, Resources, Data curation.

Declaration of competing interest

The authors declare the following financial interests/personal relationships which may be considered as potential competing interests: Eugenio Schuster reports financial support was provided by US Department of Energy. If there are other authors, they declare that they have no known competing financial interests or personal relationships that could have appeared to influence the work reported in this paper.

Acknowledgments

This material is based upon work supported by the U.S. Department of Energy, Office of Science, Office of Fusion Energy under Award Number DE-SC0021385.

Data availability

The authors do not have permission to share data.

References

[1] J. Mitchell, A. Parrott, F. Casson, F. Eriksson, F. Koechl, M. Lennholm, O. Bardsley, H. Meyer, S. Aleiferis, Scenario trajectory optimization and control on STEP, Fusion Eng. Des. 192 (2023) 113777.

[2] J. Seo, Y.-S. Na, B. Kim, C. Lee, M. Park, S. Park, Y. Lee, Development of an operation trajectory design algorithm for control of multiple 0D parameters using deep reinforcement learning in KSTAR, Nucl. Fusion 62 (8) (2022) 086049.

[3] C. Xu, Y. Ou, J. Dalessio, E. Schuster, T.C. Luce, J.R. Ferron, M.L. Walker, D.A. Humphreys, Ramp-up-phase current-profile control of tokamak plasmas via nonlinear programming, IEEE Trans. Plasma Sci. 38 (2) (2010) 163–173.

[4] B. Leard, S. Paruchuri, T. Rafiq, E. Schuster, Fast model-based scenario optimization in NSTX-U enabled by analytic gradient computation, Fusion Eng. Des. 192 (2023) 113606.

[5] J.M. Kwon, H. Choi, J. Ki, S.Y. Park, S.H. Park, Y.J. Kim, H. Cho, S. Kim, H.S. Chae, K.-S. Lee, M. Woo, T. Lee, D. Lee, J. Park, T. Tak, T. Rhee, K. Kim, H. Han, Development of a Virtual Tokamak platform, Fusion Eng. Des. 184 (2022) 113281.

[6] W. Tang, E. Feibush, G. Dong, N. Borthwick, A. Lee, J. Gomez, T. Gibbs, J. Stone, P. Messmer, J. Wells, AI-Machine Learning-Enabled Tokamak Digital Twin, 2024, arXiv preprint arXiv:2409.03112.

[7] Y. Ou, T. Luce, E. Schuster, J. Ferron, M. Walker, C. Xu, D. Humphreys, Towards model-based current profile control at DIII-D, Fusion Eng. Des. 82 (5) (2007) 1153–1160.

[8] J. Barton, M. Boyer, W. Shi, W. Wehner, E. Schuster, J. Ferron, M. Walker, D. Humphreys, T. Luce, F. Turco, B. Penaflor, R. Johnson, Physics-model-based nonlinear actuator trajectory optimization and safety factor profile feedback control for advanced scenario development in DIII-D, Nucl. Fusion 55 (9) (2015) 093005.

[9] Z. Ilhan, J. Barton, E. Schuster, D. Gates, S. Gerhardt, J. Menard, Physics-based control-oriented modeling of the current density profile evolution in NSTX-Upgrade, Fusion Eng. Des. 123 (2017) 564–568.

[10] Z. Ilhan, W. Wehner, J. Barton, E. Schuster, D. Gates, S. Gerhardt, J. Menard, First-principles-driven model-based optimal control of the current profile in NSTX-U, in: 2015 IEEE Conference on Control Applications (CCA), 0021/2015-09-23, pp. 1303–1308.

[11] A. Pajares, E. Schuster, Integrated Robust Control of the Global Toroidal Rotation and Total Plasma Energy in Tokamaks, IEEE Trans. Plasma Sci. 48 (6) (2020) 1606–1612.

[12] S. Morosohk, A. Pajares, T. Rafiq, E. Schuster, Neural network model of the multi-mode anomalous transport module for accelerated transport simulations, Nucl. Fusion 61 (10) (2021) 106040.

[13] Z. Wang, S. Morosohk, T. Rafiq, E. Schuster, M. Boyer, W. Choi, Neural network model of neutral beam injection in the EAST tokamak to enable fast transport simulations, Fusion Eng. Des. 191 (2023) 113514.

[14] H. Wang, E. Schuster, T. Rafiq, A. Kritz, S. Ding, Model-based optimal scenario planning in EAST, Fusion Eng. Des. 123 (2017) 569–573.

[15] S. Morosohk, A. Pajares, E. Schuster, Estimation of the Electron Temperature Profile in Tokamaks Using Analytical and Neural Network Models, in: 2022 American Control Conference (ACC), 2022, pp. 278–283.

[16] V. Shafranov, Equilibrium of a plasma toroid in a magnetic field, Sov. Phys. JETP 37 (10) (1960) 775.

[17] H. Grad, H. Rubin, Hydromagnetic equilibria and force-free fields, J. Nucl. Energy (1954) 7 (3–4) (1958) 284–285.

[18] Y.M. Jeon, Development of a free-boundary tokamak equilibrium solver for advanced study of tokamak equilibria, J. Korean Phys. Soc. 67 (5) (2015) 843–853.

[19] S.B. Zheng, A.J. Wootton, E.R. Solano, Analytical tokamak equilibrium for shaped plasmas, Phys. Plasmas 3 (3) (1996) 1176–1178.

[20] A. Cerfon, J. Freidberg, "One size fits all" analytic solutions to the Grad–Shafranov equation, Phys. Plasmas 17 (3) (2010) 032502.

[21] L. Guazzotto, J.P. Freidberg, Simple, general, realistic, robust, analytic tokamak equilibria. Part 1. Limiter and divertor tokamaks, 2021/05/14, J. Plasma Phys. 87 (3) (2021) 905870303.

[22] X. Song, B. Leard, Z. Wang, S.T. Paruchuri, T. Rafiq, E. Schuster, Control-Oriented Free-Boundary Equilibrium Solver for Tokamaks, Plasma 7 (4) (2024) 842–857.

[23] L.L. LoDestro, L.D. Pearlstein, On the Grad–Shafranov equation as an eigenvalue problem, with implications for q solvers, Phys. Plasmas 1 (1) (1994) 90–95.

[24] F.L. Hinton, R.D. Hazeltine, Theory of plasma transport in toroidal confinement systems, Rev. Modern Phys. 48 (1976) 239–308.

[25] M. Boyer, S. Kaye, K. Erickson, Real-time capable modeling of neutral beam injection on NSTX-U using neural networks, Nucl. Fusion 59 (5) (2019) 056008.

[26] O. Sauter, C. Angioni, Y.R. Lin-Liu, Neoclassical conductivity and bootstrap current formulas for general axisymmetric equilibria and arbitrary collisionality regime, Phys. Plasmas 6 (7) (1999) 2834–2839.

[27] V. Basiuk, J. Artaud, F. Imbeaux, X. Litaudon, A. Bécoulet, L. Eriksson, G. Hoang, G. Huysmans, D. Mazon, D. Moreau, Y. Peysson, Simulations of steady-state scenarios for Tore Supra using the CRONOS code, Nucl. Fusion 43 (9) (2003) 822.

[28] C.-S. Chang, F. Hinton, Effect of impurity particles on the finite-aspect ratio neoclassical ion thermal conductivity in a tokamak, Phys. Fluids 29 (10) (1986) 3314–3316.

[29] B. Leard, Z. Wang, S. Morosohk, T. Rafiq, E. Schuster, Fast Neural-Network Surrogate Model of the Updated Multi-Mode Anomalous Transport Module for NSTX-U, IEEE Trans. Plasma Sci. (2024) 1–7.

[30] J.D. Callen, Paleoclassical transport in low-collisionality toroidal plasmas, Phys. Plasmas 12 (9) (2005) 092512.

[31] T. Rafiq, A.Y. Pankin, G. Bateman, A.H. Kritz, F.D. Halpern, Simulation of electron thermal transport in H-mode discharges, Phys. Plasmas 16 (3) (2009) 032505.

[32] V. Graber, E. Schuster, Nonlinear burn control in ITER using adaptive allocation of actuators with uncertain dynamics, Nucl. Fusion 62 (2) (2022) 026016.

[33] R. Gross, Fusion Energy, John Wiley and Sons,New York, NY, United States, 1984.

[34] S. Gerhardt, R. Andre, J. Menard, Exploration of the equilibrium operating space for NSTX-Upgrade, Nucl. Fusion 52 (8) (2012) 083020.

[35] F. Poli, R. Andre, N. Bertelli, S. Gerhardt, D. Mueller, G. Taylor, Simulations towards the achievement of non-inductive current ramp-up and sustainment in the National Spherical Torus Experiment Upgrade, Nucl. Fusion 55 (12) (2015) 123011.

[36] T. Rafiq, C. Wilson, C. Clauser, E. Schuster, J. Weiland, J. Anderson, S. Kaye, A. Pankin, B. LeBlanc, R. Bell, Predictive modeling of NSTX discharges with the updated multi-mode anomalous transport module, Nucl. Fusion 64 (7) (2024) 076024.

[37] T. Rafiq, Z. Wang, S. Morosohk, E. Schuster, J. Weiland, W. Choi, H. Kim, Validating the Multi-Mode Model's Ability to Reproduce Diverse Tokamak Scenarios, Plasma 6 (3) (2023) 435–458.

[38] T. Rafiq, A.H. Kritz, J. Weiland, A.Y. Pankin, L. Luo, Physics basis of Multi-Mode anomalous transport module, Phys. Plasmas 20 (3) (2013) 032506.

[39] R. Goldston, D. McCune, H. Towner, S. Davis, R. Hawryluk, G. Schmidt, New techniques for calculating heat and particle source rates due to neutral beam injection in axisymmetric tokamaks, J. Comput. Phys. 43 (1) (1981) 61–78.

[40] A. Pankin, D. McCune, R. Andre, G. Bateman, A. Kritz, The tokamak Monte Carlo fast ion module NUBEAM in the National Transport Code Collaboration library, Comput. Phys. Comm. 159 (3) (2004) 157–184.

[41] R. Hawryluk, An empirical approach to Tokamak transport, in: B. Coppi, G. Leotta, D. Pfirsch, R. Pozzoli, E. Sindoni (Eds.), Physics of Plasmas Close To Thermonuclear Conditions, Pergamon, 1981, pp. 19–46.